Plasmon-Enhanced Nonlinear Wave Mixing in Nanostructured Graphene

Joel D. Cox[*,†] and F. Javier García de Abajo[*,†,‡]

[†]ICFO-Institut de Ciencies Fotoniques, Mediterranean Technology Park, 08860 Castelldefels, Barcelona, Spain
[‡]ICREA-Institució Catalana de Recerca i Estudis Avançats, Passeig Lluís Companys 23, 08010 Barcelona, Spain

S *Supporting Information*

ABSTRACT: Localized plasmons in metallic nanostructures have been widely used to enhance nonlinear optical effects due to their ability to concentrate and enhance light down to extreme-subwavelength scales. As alternatives to noble metal nanoparticles, graphene nanostructures can host long-lived plasmons that efficiently couple to light and are actively tunable via electrical doping. Here we show that doped graphene nanoislands present unique opportunities for enhancing non-linear optical wave-mixing processes between two externally applied optical fields at the nanoscale. These small islands can

support pronounced plasmons at multiple frequencies, resulting in extraordinarily high wave-mixing susceptibilities when one or more of the input or output frequencies coincide with a plasmon resonance. By varying the doping charge density in a nanoisland with a fixed geometry, enhanced wave mixing can be realized over a wide spectral range in the visible and near-infrared. We concentrate, in particular, on second- and third-order processes, including sum and difference frequency generation, as well as on four-wave mixing. Our calculations for armchair graphene triangles composed of up to several hundred carbon atoms display large wave mixing polarizabilities compared with metal nanoparticles of similar lateral size, thus supporting nanographene as an excellent material for tunable nonlinear optical nanodevices.

KEYWORDS: *nonlinear optics/plasmonics, nanographene, active plasmonics, wave mixing, sum/difference frequency generation, four-wave mixing*
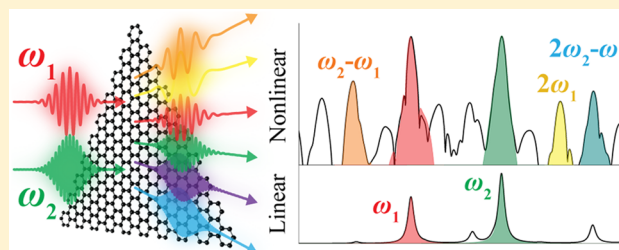
Nonlinear optical phenomena arise from the coupling between two or more photons, mediated by their interaction with matter, to produce a photon with a frequency that is a linear combination of the original photon frequencies. These processes are responsible for many significant advances in laser-based technologies,[1,2] most of which rely on phase-matching of intense electromagnetic fields in extended bulk crystalline media to enable efficient frequency conversion. Now, as the accessibility of nanostructured materials offered by modern nanofabrication techniques continues to increase, so does the interest in mastering nonlinear optics on subwavelength scales. Indeed, nonlinear optical nanomaterials find diverse applications, including optical microscopy,[3,4] biological imaging/detection,[5,6] and signal conversion in nanoscale photonic devices.[7–10]

Inherently, nanostructured materials possess small volumes that limit their interaction with optical fields. Fortunately, this can be compensated by high oscillator strengths provided by either quantum confinement effects[11] or the intense near-fields generated by localized surface plasmons.[7,12] In particular, the near-field enhancement associated with plasmons in noble metal nanostructures has been widely used with the purpose of enhancing the nonlinear response of composites formed by embedding them in surrounding dielectric materials.[9,10,13]

Plasmons also display strong intrinsic optical nonlinearities, clearly observed in metal nanoparticles.[13–16]

The plasmonic response of a metal nanostructure can be tailored by its size, shape, and surrounding environment,[12] as well as by combining two or more interacting particles. In this manner, a metallic nanocomposite can be engineered to possess multiple resonance frequencies, enabling the optimization of nonlinear wave mixing between multifrequency optical fields.[17,18] Unfortunately, plasmons are hardly tunable in metals after a structure has been fabricated,[19] thus severely limiting the choice of frequency combinations.

As an alternative plasmonic material, electrically doped graphene has been found to support long-lived plasmonic excitations that efficiently couple to light and are actively tunable by changing the density of charge carriers.[20–32] Strong intrinsic nonlinearities have also been observed in this material,[33–35] which could be further enhanced by plasmons.[36,37] Recently, plasmon-assisted second-harmonic generation (SHG) and down conversion with good efficiencies at the few-photon level have been argued to be possible when the fundamental and the second-harmonic are simultaneously resonant with plasmons in a graphene nanoisland.[38] We have
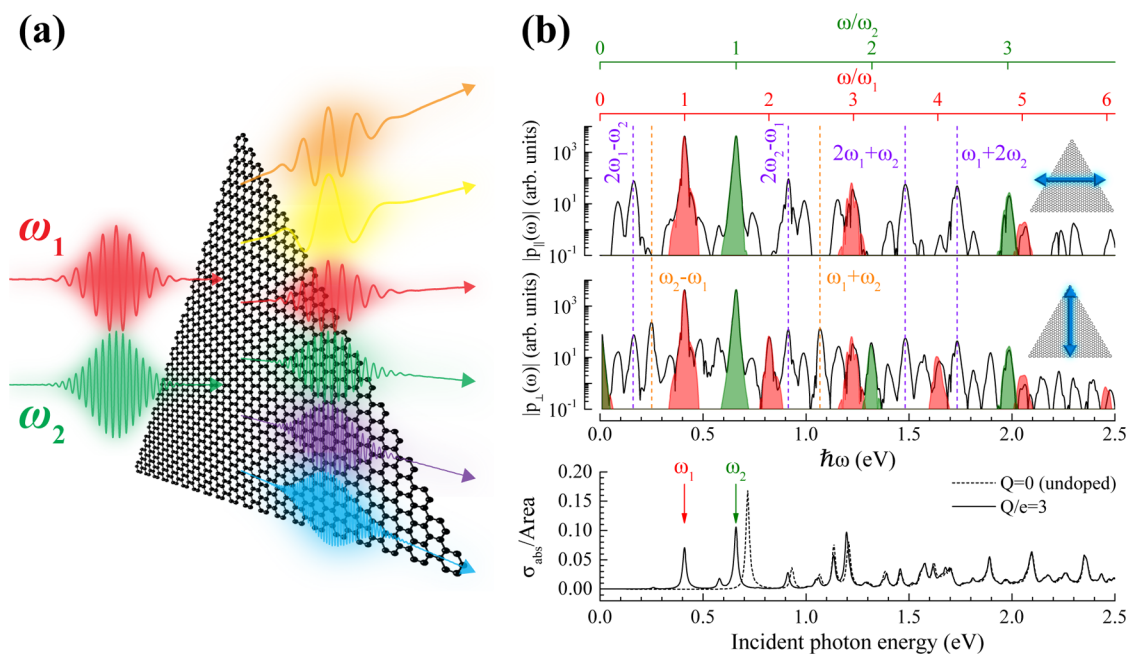
Figure 1. Plasmon-enhanced wave mixing of coincident pulses. (a) Illustration of an armchair triangular graphene nanoisland containing $N = 1260$ carbon atoms (side length of 8.4 nm) and doped with charge $Q = 3e$, illuminated by two collinear light pulses of central energies $\hbar\omega_1 = 0.41$ eV and $\hbar\omega_2 = 0.66$ eV, each having 200 fs fwhm duration and peak intensity 10^{12} W/m^2. (b) Spectral density of the induced dipole moment under excitation by light polarized along a direction parallel (upper panel) or perpendicular (middle panel) to one of the nanotriangle sides (dipole along the incident electric-field direction). The solid black curves correspond to the spectra obtained upon excitation by coincident pulses, while the filled curves show the spectra produced by individual pulses of central frequency ω_1 (red) or ω_2 (green). The linear absorption cross-section of the nanoisland (normalized to its area) is presented in the lower panel (solid curve), where the arrows indicate the central frequencies of the exciting pulses and we compare it with the absorption of the undoped island (dashed curve).

predicted that a similar mechanism can lead to unprecedentedly intense SHG and third-harmonic generation (THG) in nanographene.[39] Although experimental studies have so far demonstrated strong plasmons only at mid-infrared and terahertz frequencies,[20−30] further reduction in the size of the islands down to less than 10 nm should allow us to reach the visible and near-infrared (vis-NIR) regimes.[32,40−42] In particular, commercially available polycyclic aromatic molecules sustain plasmon-like resonances that are switched on and off by changing their charge state.[42] Additionally, recent progress in the chemical synthesis of nanographene[43−47] provides further stimulus for the use of this material to produce electrically tunable vis-NIR plasmons, as well as their application to nonlinear optics at the nanoscale.

In this work, we investigate nonlinear optical wave mixing in doped nanographene. Specifically, we propose a scheme for optimizing wave mixing among multifrequency optical fields that utilizes the plasmons supported by a doped graphene nanoisland. Using a tight-binding description for the electronic structure combined with density-matrix quantum-mechanical simulations, we demonstrate that efficient wave mixing is achieved in an island when the incident and the mixed frequencies are coupled with one or more of its plasmons. By actively tuning the doping level in a graphene nanoisland of fixed geometry, a wide range of plasmon-enhanced input/output mixing frequency combinations can be realized.

We study wave mixing of coincident light pulses in Figure 1 for a triangular armchair-edged graphene nanoisland containing $N = 1260$ carbon atoms (side length of 8.4 nm) and doped with three electrons (doping density 9.1×10^{12} cm^{-2}, corresponding to an equivalent extended graphene Fermi energy $E_F = 0.35$ eV). Additionally, we assume a conservative inelastic lifetime τ

$= 33$ fs (i.e., line width $\hbar\tau^{-1} = 20$ meV). From the linear absorption cross-section of the nanoisland, we identify several prominent plasmons at specific incident photon energies. In particular, we concentrate on $\hbar\omega_1 = 0.41$ eV and $\hbar\omega_2 = 0.66$ eV. The first of these plasmons is highly tunable upon electrical doping, as it is switched on when moving from $Q = 0$ to $Q \neq 0$ charge states (see lower panel in Figure 1b), and its frequency increases with Q (see Supporting Information, SI, Figure S1). The plasmon at ω_2 is comparatively less tunable. Plasmon-enhanced optical wave mixing in the nanoisland is demonstrated in Figure 1b, where the spectral decomposition of the induced dipole moment is shown for excitation by collinear Gaussian pulses with central frequencies ω_1 and ω_2. We show the response for incident polarization aligned with an edge of the nanoisland (upper panels) or perpendicular to an edge (middle panels), and in each case the dipole is calculated along the direction of polarization. Additionally, in Figure 1b we superimpose the spectra obtained from coincident pulses with the spectra for excitation of the nanoisland by each of the individual pulses in isolation, which exhibit polarization features that oscillate at harmonics of the fundamental frequencies ($n\omega_1$ and $n\omega_2$). The dual-pulse spectrum exhibits these features in addition to polarization components produced via sum and difference frequency generation ($\omega_1 \pm \omega_2$) and degenerate four-wave mixing ($\omega_1 \pm 2\omega_2$ or $2\omega_1 \pm \omega_2$), along with various other combinations of harmonic generation and wave mixing. We note that for polarization along the edge of a nanotriangle, inversion symmetry in this direction prevents even-ordered nonlinear processes from occurring, such as SHG and sum/ difference frequency generation. Incidentally, mixing of less tunable plasmons (e.g., $\hbar\omega_2$ with the resonance at 1.20 eV)
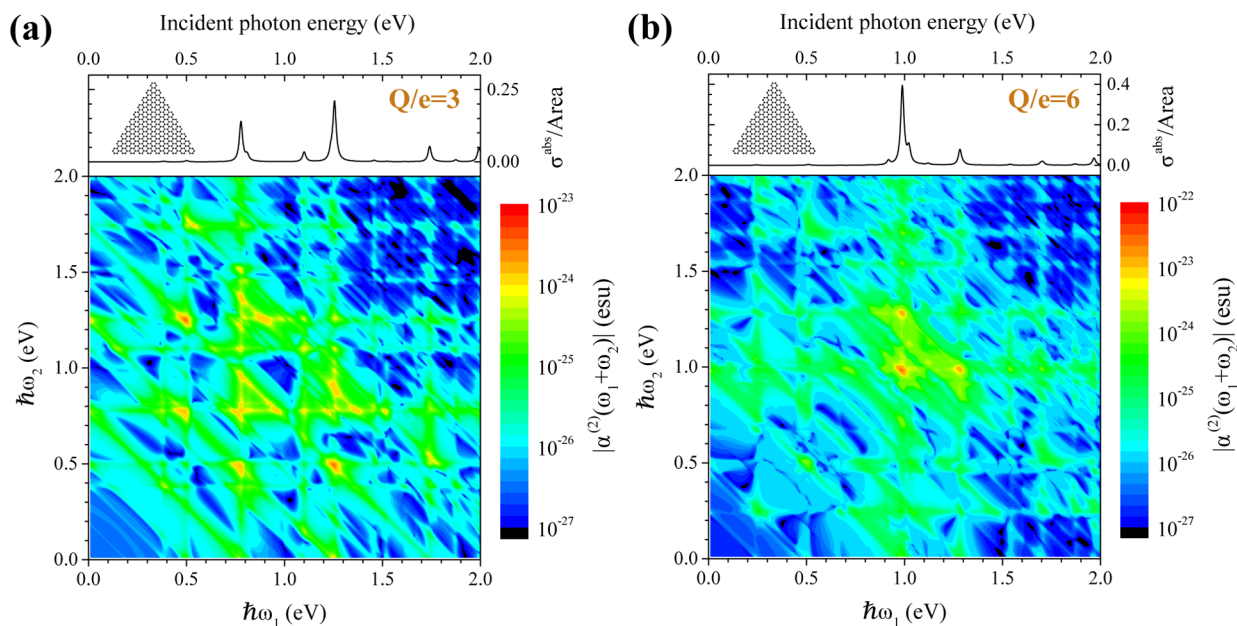
Figure 2. Sum frequency generation. We show the nonlinear polarizability $\alpha^{(2)}(\omega_1 + \omega_2)$, corresponding to sum-frequency generation (SFG), for an armchair-edged triangular graphene nanoisland containing $N = 330$ carbon atoms and doped with (a) three and (b) six additional electrons. The upper plots show the linear absorption cross-section, while the lower panels show the polarizabilities as the incident field frequencies ω_1 and ω_2 are varied.
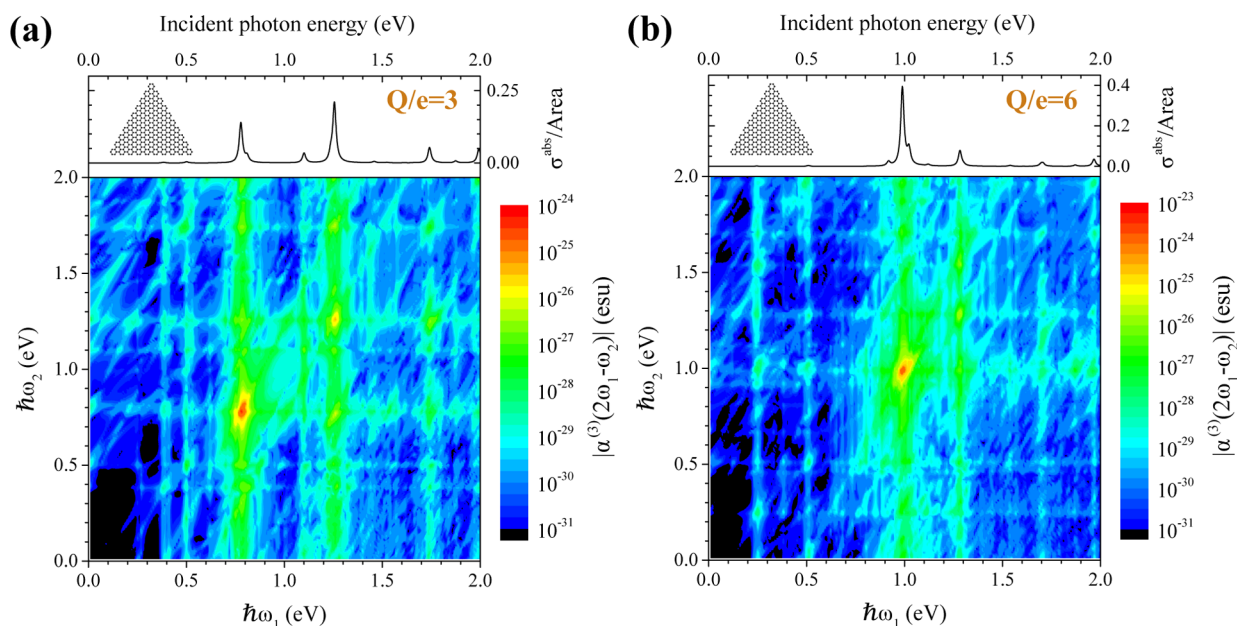
Figure 3. Four-wave mixing. We show the nonlinear polarizability $\alpha^{(3)}(2\omega_1 - \omega_2)$, corresponding to four-wave mixing, for the same nanoisland and doping conditions considered in Figure 2

generally produces less intense nonlinear features (see Figure S2 in SI).

While the response of a graphene nanoisland to ultrashort pulses can provide information on the relative strengths of the nonlinear processes for excitation at specific frequencies, a quantitative analysis of each nonlinear process, along with its optimal plasmonic enhancement, is best provided by studying the response under continuous-wave (cw) illumination. In Figure 2 we consider sum-frequency generation (SFG) in a nanoisland containing $N = 330$ atoms (side length of 4.4 nm), for doping with either three (Figure 2a) or six (Figure 2b) additional charge carriers. The upper panels in Figure 2 show

the linear response of the nanoisland for the two doping levels considered, which show multiple plasmon resonance peaks at low doping that converge to a single, stronger feature as the doping level increases. The SFG polarizability $\alpha^{(2)}(\omega_1 + \omega_2)$ is presented as a function of the two applied field frequencies, enabling exploration of all possible frequency combinations that may result in plasmon-enhanced wave mixing.

The input frequencies at which SFG is enhanced are found to coincide with the plasmons, corresponding to the horizontally and vertically aligned features in the contour plot of $|\alpha^{(2)}(\omega_1 + \omega_2)|$ in Figure 2. Strong enhancement is observed where these features intersect, driven by plasmons excited at both
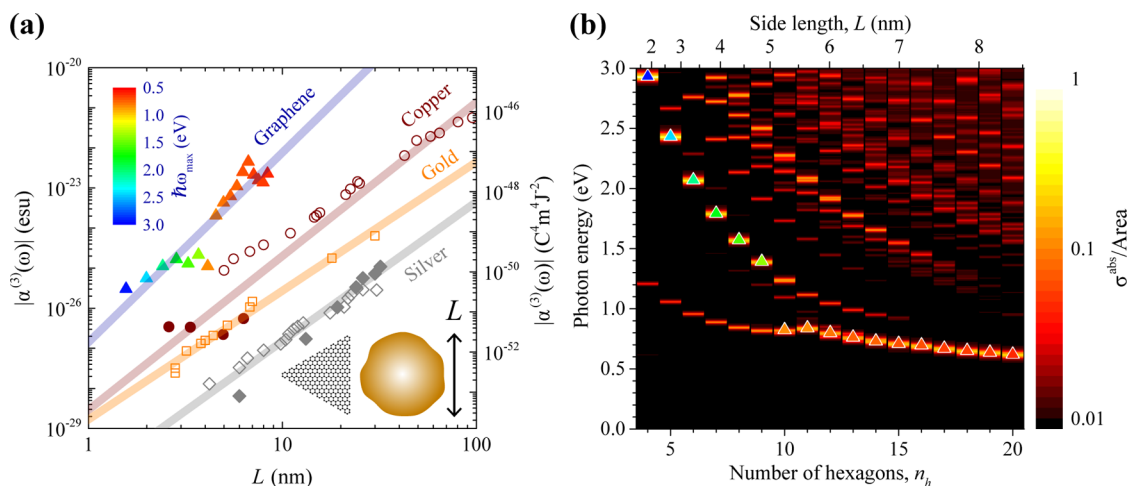
Figure 4. Third-order response of nanographene compared to that of noble metal nanoparticles. (a) The maximum nonlinear polarizabilities $\alpha^{(3)}(\omega)$ of graphene nanoislands (solid triangles) as a function of their side length L are compared with measured values of noble metal nanoparticles of similar diameter reported in the literature. The color scale indicates the incident photon energy at which the maximum graphene nonlinear polarizabilities are found. The semitransparent solid lines are guides to the eye, added to indicate the scaling with L. (b) Linear absorption spectra for the armchair-edged graphene nanotriangles considered in (a), distinguished by the number of hexagons along the edge n_h, for which a fixed doping density of one electron per 100 carbon atoms is maintained. The frequencies at which the maximum values of $\alpha^{(3)}(\omega)$ occur are indicated by the solid triangles, which follow the color scale in (a). The experimental data used in (a) is extracted from refs 48−51, where the polarizabilities are obtained upon multiplication of the reported third-order susceptibility $|\chi^{(3)}|$ by the particle volume. Specifically, we show data obtained via fully degenerate four-wave mixing measurements of several noble metals performed at different wavelengths: gold nanoparticles at ∼530 nm[48] (hollow squares), silver nanoparticles at ∼420 nm[49] (hollow diamonds) and near ∼410 nm[51] (solid diamonds), and copper nanoparticles at ∼570 nm[49] (hollow circles) and ∼530 nm[50] (solid circles).

fundamental frequencies. Prominent features also follow frequencies satisfying $\omega_2 + \omega_1 = \omega_p$, where ω_p denotes one of the plasmon frequencies of the nanoisland, indicating plasmonic enhancement at the output (sum) frequency. Finally, since SHG can be considered as a special case of SFG, we also note plasmonic enhancement of SHG for frequencies satisfying $\omega_1 = \omega_2 = \omega_p$.

Similar conclusions are drawn from frequency-difference generation (i.e., $\alpha^{(2)}(\omega_1 - \omega_2)$), where we observe enhancement when either one of the incident frequencies or the output frequency resonates with a plasmon (see Figure S3 in SI).

Plasmonic enhancement of four-wave mixing is investigated in Figure 3 for the same graphene nanoisland and doping conditions considered for Figure 2, with an output frequency $2\omega_1 - \omega_2$. We find enhancement in $\alpha^{(3)}(2\omega_1 - \omega_2)$ when either of the fundamental frequencies of the incident fields are resonant with plasmons in the nanoisland, although in this case the enhancement favors $\omega_1 = \omega_p$, as ω_1 is involved twice in these specific wave mixing processes. Here we find increased four-wave mixing following the frequencies $\omega_2 = 2\omega_1 - \omega_p$, once again indicating enhancement at the output frequency. For $\omega_1 = \omega_2$ we have fully degenerate four-wave mixing, where we are actually investigating the third-order polarizability $\alpha^{(3)}(\omega_1)$ contributing to the linear response (i.e., the Kerr effect). In this case, frequencies satisfying the condition $\omega_1 = \omega_2 = \omega_p$ produce extremely high polarizabilities, as the three input frequencies and the output frequency are all equally amplified by the same plasmon resonance. We have also examined four-wave mixing with output frequency $2\omega_1 + \omega_2$, leading to similar conclusions on plasmon-assisted enhancement (see Figure S4 in SI).

As noble metal nanoparticles possess the highest nonlinear polarizabilities per atom measured experimentally,[13] we compare them with the above results for doped nanographene nonlinear polarizabilities. In particular, we contrast data

available in the literature for metal third-order polarizabilities $\alpha^{(3)}(\omega)$ with those calculated here for graphene. In Figure 4a we show the maximum polarizability $|\alpha^{(3)}(\omega)|$ for graphene nanoislands of increasing size, and for a fixed doping ratio of one electron per every hundred carbon atoms, along with experimental data obtained from degenerate four-wave mixing experiments on gold, silver, and copper nanoparticles of comparable or greater sizes. Even through metal particles have much larger volumes than graphene nanoislands for a given lateral size L, we find the latter to exhibit much larger nonlinear response, reaching 2 orders of magnitude higher values. Obviously, we are comparing theory for graphene with experiments for metals, so this is a preliminary conclusion, which should be examined experimentally. Nonetheless, we are using a conservative inelastic lifetime for nanographene in our calculations ($\tau = 33$ fs), whereas much longer lifetimes could be actually encountered in practice, based upon recently measured plasmon resonances,[26,52] and it should be noted that the nonlinear polarizability of order n scales roughly as τ^n.[39] The linear absorption spectra for the nanoislands that we compare with metal nanoparticles are presented in Figure 4b, illustrating how the plasmon resonances vary as the nanoisland size increases while a fixed doping density is maintained.

In conclusion, graphene nanoislands can be used to realize nonlinear wave mixing on the nanoscale with extraordinarily high efficiencies, surpassing those of metal nanoparticles of similar lateral sizes. The large magnitudes of the predicted nonlinear polarizabilities are attributed to plasmonic enhancement in these nanostructures. Wave mixing is further enhanced by simultaneously exploiting multiple plasmonic resonances, enabling two incident fields with distinct frequencies to independently couple to plasmons, and additionally tuning the mixed frequency to yet another plasmon. These plasmons can be tuned by changing the number of doping charge carriers, adding another advantage with respect to conventional

plasmonic metal response. Interestingly, by considering islands formed by a few hundreds or thousands of carbon atoms, we predict tunable plasmonic response and plasmon-induced enhanced nonlinearities within the visible and near-infrared spectral ranges. Our results configure a new platform for the development of nanoscale nonlinear optical devices based upon graphene nanostructures with lateral dimensions of only a few nanometers, such as those that are currently produced by chemical synthesis.[43−47]

■ METHODS

We describe the low-energy (<3 eV) optical response of graphene nanoislands within a density-matrix approach, using a tight-binding model for the π-band electronic structure.[53,54] One-electron states $|\varphi_j\rangle$ are obtained by assuming a single p orbital per carbon site, oriented perpendicular to the graphene plane, with a hopping energy of 2.8 eV between nearest neighbors. In the spirit of the mean-field approximation,[55] a single-particle density matrix is constructed as $\rho = \sum_{jj'}\tilde{\rho}_{jj'}|\varphi_j\rangle\langle\varphi_{j'}|$, where $\tilde{\rho}_{jj'}$ are time-dependent complex numbers. An incoherent Fermi−Dirac distribution of occupation fractions f_j is assumed in the unperturbed state, characterized by a density matrix $\tilde{\rho}_{jj'}^0 = \delta_{jj'}f_j$, whereas the time evolution under external illumination is governed by the equation of motion

$$\frac{\partial \rho}{\partial t} = -\frac{i}{\hbar}[H, \rho] - \frac{1}{2\tau}(\rho - \rho^0) \tag{1}$$

The last term of eq 1 describes inelastic losses at a phenomenological decay rate $1/\tau$. We set $\hbar\tau^{-1} = 20$ meV throughout this work (i.e., $\tau = 33$ fs), corresponding to a conservative Drude-model graphene mobility $\mu \approx 460$ cm^2 V^{-1} s^{-1} for a characteristic doping carrier density 4×10^{13} cm^{-2} (i.e., one charge carrier per every 100 carbon atoms). The system Hamiltonian $H = H_{TB} - e\phi$ consists of the tight-binding part H_{TB} (i.e., nearest-neighbors hopping) and the interaction with the self-consistent electric potential ϕ, which is in turn the sum of external and induced potentials. The latter is simply taken as the Hartree potential produced by the perturbed electron density, while the former reduces to $-\mathbf{r}\cdot\mathbf{E}(t)$ for an incident electric field $\mathbf{E}(t)$. The induced dipole moment is then calculated from the diagonal elements of the density matrix in the carbon-site representation as $\mathbf{p}(t) = -2e\sum_l[\rho_{ll}(t) - \rho_{ll}^0]\mathbf{R}_l$, where the factor of 2 accounts for spin degeneracy and $\mathbf{R}_l = (x_l, y_l)$ runs over carbon sites.

We use two different methods to solve eq 1 and find $\mathbf{p}(t)$ (direct time-domain numerical integration and a perturbative approach[39]), which we find in excellent mutual agreement under low-intensity cw illumination. Direct time integration allows us to simulate the response to short light pulses for arbitrarily large intensity, while the perturbative method yields the nonlinear polarizabilities under multifrequency cw illumination ($\mathbf{E}(t) = E_0\hat{\mathbf{e}}e^{-i\omega_1 t} + E_0\hat{\mathbf{e}}e^{-i\omega_2 t} +$ c.c., with the same amplitude E_0 at both frequencies for simplicity), for which we can express the dipole moment as a power series in the electric field strength E_0 according to

$$p(t) = \sum_n \sum_{s_1=-n}^{n} \sum_{s_2=-n}^{n} \alpha^{(n)}(s_1\omega_1 + s_2\omega_2)(E_0)^n e^{-i(s_1\omega_1 + s_2\omega_2)t}$$
$$+ \text{ c.c.} \tag{2}$$

Here, n is the scattering order, whereas s_1 and s_2 give the harmonic orders of the incident frequencies ω_1 and ω_2. We

denote polarizabilities according to $\alpha^{(n)}(\omega_{out})$, where ω_{out} is the frequency generated by a particular n^{th}-order process. Considering terms up to third order ($n \leq 3$), eq 2 then defines the linear polarizability $\alpha^{(1)}(\omega_i)$ ($i = 1$ or 2), the polarizabilities for SHG and THG, $\alpha^{(2)}(2\omega_i)$ and $\alpha^{(3)}(3\omega_i)$, respectively, the wave-mixing polarizabilities corresponding to sum and difference frequency generation $\alpha^{(2)}(\omega_i \pm \omega_j)$ ($j = 1$ or 2, $i \neq j$), and the four-wave mixing polarizabilities $\alpha^{(3)}(2\omega_i \pm \omega_j)$ and $\alpha^{(3)}(\omega_i + \omega_j - \omega_j)$. We obtain these polarizabilities by expanding the density matrix in eq 1 as

$$\rho = \sum_n \sum_{s_1=-n}^{n} \sum_{s_2=-n}^{n} \rho^{ns_1s_2} e^{-i(s_1\omega_1 + s_2\omega_2)t} \tag{3}$$

which leads to self-consistent equations in $\rho^{ns_1s_2}$ (for the relevant combinations of n with harmonics s_1 and s_2). We solve eq 3 following a procedure inspired in the random-phase approximation (RPA) formalism, as discussed elsewhere[39] for SHG and THG. Further details on the extension of this formalism to cope with wave mixing are given in the SI.

■ ASSOCIATED CONTENT

⑤ Supporting Information
Details of the theoretical formalism and additional supporting data. This material is available free of charge via the Internet at http://pubs.acs.org.

■ AUTHOR INFORMATION

Corresponding Authors
*E-mail: joel.cox@icfo.es.
*E-mail: javier.garciadeabajo@icfo.es.

Notes
The authors declare no competing financial interest.

■ REFERENCES

(1) Boyd, R. W. *Nonlinear Optics*, 3rd ed.; Academic Press: Amsterdam, 2008.
(2) Garmire, E. Nonlinear optics in daily life. *Opt. Express* **2013**, *21*, 30532−30544.
(3) Wang, Y.; Lin, C.-Y.; Nikolaenko, A.; Raghunathan, V.; Potma, E. O. Four-wave mixing microscopy of nanostructures. *Adv. Opt. Photon.* **2011**, *3*, 1−52.
(4) Huang, L.; Cheng, J.-X. Nonlinear optical microscopy of single nanostructures. *Annu. Rev. Mater. Res.* **2013**, *43*, 213−236.
(5) Pu, Y.; Grange, R.; Hsieh, C.-L.; Psaltis, D. Nonlinear optical properties of core-shell nanocavities for enhanced second-harmonic generation. *Phys. Rev. Lett.* **2010**, *104*, 207402.
(6) Pantazis, P.; Maloney, J.; Wu, D.; Fraser, S. E. Second harmonic generating (SHG) nanoprobes for in vivo imaging. *Proc. Natl. Acad. Sci. U.S.A.* **2010**, *107*, 14535−14540.
(7) Novotny, L.; Van Hulst, N. Antennas for light. *Nat. Photonics* **2011**, *5*, 83−90.
(8) Chen, P.-Y.; Argyropoulos, C.; Alù, A. Enhanced nonlinearities using plasmonic nanoantennas. *Nanophotonics* **2012**, *1*, 221−233.
(9) Aouani, H.; Rahmani, M.; Navarro-Cía, M.; Maier, S. A. Third-harmonic-upconversion enhancement from a single semiconductor nanoparticle coupled to a plasmonic antenna. *Nat. Nanotechnol.* **2014**, *9*, 290−294.
(10) Metzger, B.; Hentschel, M.; Schumacher, T.; Lippitz, M.; Ye, X.; Murray, C. B.; Knabe, B.; Buse, K.; Giessen, H. Doubling the efficiency

of third harmonic generation by positioning ITO nanocrystals into the hot-spot of plasmonic gap-antennas. *Nano Lett.* **2014**, *14*, 2867−2872.

(11) Alivisatos, A. P. Semiconductor clusters, nanocrystals, and quantum dots. *Science* **1996**, *271*, 933−937.

(12) Stockman, M. I. Nanoplasmonics: The physics behind the applications. *Phys. Today* **2011**, *64*, 39−44.

(13) Kauranen, M.; Zayats, A. V. Nonlinear plasmonics. *Nat. Photonics* **2012**, *6*, 737−748.

(14) Danckwerts, M.; Novotny, L. Optical frequency mixing at coupled gold nanoparticles. *Phys. Rev. Lett.* **2007**, *98*, 026104.

(15) Palomba, S.; Danckwerts, M.; Novotny, L. Nonlinear plasmonics with gold nanoparticle antennas. *J. Opt. A: Pure Appl. Opt.* **2009**, *11*, 114030.

(16) Valev, V. K. Characterization of nanostructured plasmonic surfaces with second harmonic generation. *Langmuir* **2012**, *28*, 15454−15471.

(17) Harutyunyan, H.; Volpe, G.; Quidant, R.; Novotny, L. Enhancing the nonlinear optical response using multifrequency gold-nanowire antennas. *Phys. Rev. Lett.* **2012**, *108*, 217403.

(18) Nordlander, Y. Z. F. W. Y.-R. Z. P.; Halas, N. J. Coherent Fano resonances in a plasmonic nanocluster enhance optical four-wave mixing. *Proc. Natl. Acad. Sci. U.S.A.* **2013**, *110*, 9215−9219.

(19) Novotny, L.; Hecht, B. *Principles of Nano-Optics*; Cambridge University Press: New York, 2006.

(20) Ju, L.; Geng, B.; Horng, J.; Girit, C.; Martin, M.; Hao, Z.; Bechtel, H. A.; Liang, X.; Zettl, A.; Shen, Y. R.; et al. Graphene plasmonics for tunable terahertz metamaterials. *Nat. Nanotechnol.* **2011**, *6*, 630−634.

(21) Fei, Z.; Andreev, G. O.; Bao, W.; Zhang, L. M.; McLeod, A. S.; Wang, C.; Stewart, M. K.; Zhao, Z.; Dominguez, G.; Thiemens, M.; et al. Infrared nanoscopy of Dirac plasmons at the graphene−SiO$_2$ interface. *Nano Lett.* **2011**, *11*, 4701−4705.

(22) Chen, J.; Badioli, M.; Alonso-González, P.; Thongrattanasiri, S.; Huth, F.; Osmond, J.; Spasenović, M.; Centeno, A.; Pesquera, A.; Godignon, P.; et al. Optical nano-imaging of gate-tunable graphene plasmons. *Nature* **2012**, *487*, 77−81.

(23) Fei, Z.; Rodin, A. S.; Andreev, G. O.; Bao, W.; McLeod, A. S.; Wagner, M.; Zhang, L. M.; Zhao, Z.; Thiemens, M.; Dominguez, G.; et al. Gate-tuning of graphene plasmons revealed by infrared nano-imaging. *Nature* **2012**, *487*, 82−85.

(24) Yan, H.; Li, X.; Chandra, B.; Tulevski, G.; Wu, Y.; Freitag, M.; Zhu, W.; Avouris, P.; Xia, F. Tunable infrared plasmonic devices using graphene/insulator stacks. *Nat. Nanotechnol.* **2012**, *7*, 330−334.

(25) Yan, H.; Li, Z.; Li, X.; Zhu, W.; Avouris, P.; Xia, F. Infrared spectroscopy of tunable Dirac terahertz magneto-plasmons in graphene. *Nano Lett.* **2012**, *12*, 3766−3771.

(26) Fang, Z.; Thongrattanasiri, S.; Schlather, A.; Liu, Z.; Ma, L.; Wang, Y.; Ajayan, P. M.; Nordlander, P.; Halas, N. J.; García de Abajo, F. J. Gated tunability and hybridization of localized plasmons in nanostructured graphene. *ACS Nano* **2013**, *7*, 2388−2395.

(27) Brar, V. W.; Jang, M. S.; Sherrott, M.; Lopez, J. J.; Atwater, H. A. Highly confined tunable mid-infrared plasmonics in graphene nanoresonators. *Nano Lett.* **2013**, *13*, 2541−2547.

(28) Fang, Z.; Wang, Y.; Schlather, A.; Liu, Z.; Ajayan, P. M.; García de Abajo, F. J.; Nordlander, P.; Zhu, X.; Halas, N. J. Active tunable absorption enhancement with graphene nanodisk arrays. *Nano Lett.* **2014**, *14*, 299−304.

(29) Yan, H.; Low, T.; Zhu, W.; Wu, Y.; Freitag, M.; Li, X.; Guinea, F.; Avouris, P.; Xia, F. Damping pathways of mid-infrared plasmons in graphene nanostructures. *Nat. Photonics* **2013**, *7*, 394−399.

(30) Freitag, M.; Low, T.; Zhu, W.; Yan, H.; Xia, F.; Avouris, P. Photocurrent in graphene harnessed by tunable intrinsic plasmons. *Nat. Commun.* **2014**, *4*, 1951.

(31) Grigorenko, A. N.; Polini, M.; Novoselov, K. S. Graphene plasmonics. *Nat. Photonics* **2012**, *6*, 749−758.

(32) García de Abajo, F. J. Graphene plasmonics: Challenges and opportunities. *ACS Photonics* **2014**, *1*, 135−152.

(33) Hendry, E.; Hale, P. J.; Moger, J.; Savchenko, A. K.; Mikhailov, S. A. Coherent nonlinear optical response of graphene. *Phys. Rev. Lett.* **2010**, *105*, 097401.

(34) Zhang, H.; Virally, S.; Bao, Q.; Ping, L. K.; Massar, S.; Godbout, N.; Kockaert, P. Z-scan measurement of the nonlinear refractive index of graphene. *Opt. Lett.* **2012**, *37*, 1856−1858.

(35) Kumar, N.; Kumar, J.; Gerstenkorn, C.; Wang, R.; Chiu, H.-Y.; Smirl, A. L.; Zhao, H. Third harmonic generation in graphene and few-layer graphite films. *Phys. Rev. B* **2013**, *87*, 121406(R).

(36) Mikhailov, S. A. Theory of the giant plasmon-enhanced second-harmonic generation in graphene and semiconductor two-dimensional electron systems. *Phys. Rev. B* **2011**, *84*, 045432.

(37) Gullans, M.; Chang, D. E.; Koppens, F. H. L.; García de Abajo, F. J.; Lukin, M. D. Single-photon nonlinear optics with graphene plasmons. *Phys. Rev. Lett.* **2013**, *111*, 247401.

(38) Manzoni, M. T.; Silveiro, I.; García de Abajo, F. J.; Chang, D. E. Second-order quantum nonlinear optical processes in graphene nanostructures. *arXiv:1406.4360*.

(39) Cox, J. D.; García de Abajo, F. J. Electrically tunable nonlinear plasmonics in graphene nanoislands. *Nat. Commun.* **2014**, *5*, 5725.

(40) Thongrattanasiri, S.; Manjavacas, A.; García de Abajo, F. J. Quantum finite-size effects in graphene plasmons. *ACS Nano* **2012**, *6*, 1766−1775.

(41) Manjavacas, A.; Thongrattanasiri, S.; García de Abajo, F. J. Plasmons driven by single electrons in graphene nanoislands. *Nanophotonics* **2013**, *2*, 139−151.

(42) Manjavacas, A.; Marchesin, F.; Thongrattanasiri, S.; Koval, P.; Nordlander, P.; Sánchez-Portal, D.; García de Abajo, F. J. Tunable molecular plasmons in polycyclic aromatic hydrocarbons. *ACS Nano* **2013**, *7*, 3635−3643.

(43) Wu, J.; Pisula, W.; Müllen, K. Graphenes as potential material for electronics. *Chem. Rev.* **2007**, *107*, 718−747.

(44) Feng, X.; Liu, M.; Pisula, W.; Takase, M.; Li, J.; Müllen, K. Supramolecular organization and photovoltaics of triangle-shaped discotic graphenes with swallow-tailed alkyl substituents. *Adv. Mater.* **2008**, *20*, 2684−2689.

(45) Feng, X.; Pisula, W.; Müllen, K. Large polycyclic aromatic hydrocarbons: Synthesis and discotic organization. *Pure Appl. Chem.* **2009**, *81*, 2203−2224.

(46) Cai, J.; Ruffieux, P.; Jaafar, R.; Bieri, M.; Braun, T.; Blankenburg, S.; Muoth, M.; Seitsonen, A. P.; Saleh, M.; Feng, X.; et al. Atomically precise bottom-up fabrication of graphene nanoribbons. *Nature* **2010**, *466*, 470−473.

(47) Denk, R.; Hohage, M.; Zeppenfeld, P.; Cai, J.; Pignedoli, C. A.; Söde, H.; Fasel, R.; Feng, X.; Müllen, K.; Wang, S.; et al. Exciton-dominated optical response of ultra-narrow graphene nanoribbons. *Nat. Commun.* **2014**, *5*, 4253.

(48) Hache, F.; Ricard, D.; Flytzanis, C.; Kreibig, U. The optical Kerr effect in small metal particles and metal colloids: The case of gold. *Appl. Phys. A: Mater. Sci. Process.* **1988**, *47*, 347−357.

(49) Uchida, K.; Kaneko, S.; Omi, S.; Hata, C.; Tanji, H.; Asahara, Y.; Ikushima, A. J.; Tokizaki, T.; Nakamura, A. Optical nonlinearities of a high concentration of small metal particles dispersed in glass: Copper and silver particles. *J. Opt. Soc. Am. B* **1994**, *11*, 1236−1243.

(50) Yang, L.; Becker, K.; Smith, F. M.; M, R. H., III; R.F. Haglund, J.; Yang, L.; Dorsinville, R.; Alfano, R. R.; Zuhr, R. A. Size dependence of the third-order susceptibility of copper nanoclusters investigated by four-wave mixing. *J. Opt. Soc. Am. B* **1994**, *11*, 457−461.

(51) Sato, R.; Ohnuma, M.; Oyoshi, K.; Takeda, Y. Experimental investigation of nonlinear optical properties of Ag nanoparticles: Effects of size quantization. *Phys. Rev. B* **2014**, *90*, 125417.

(52) Woessner A. et al. Highly confined low-loss plasmons in graphene-boron nitride heterostructures. *arXiv:1409.5674*.

(53) Wallace, P. R. The band theory of graphite. *Phys. Rev.* **1947**, *71*, 622−634.

(54) Castro Neto, A. H.; Guinea, F.; Peres, N. M. R.; Novoselov, K. S.; Geim, A. K. The electronic properties of graphene. *Rev. Mod. Phys.* **2009**, *81*, 109−162.

(55) Hedin, L.; Lundqvist, S. Effects of electron–electron and electron–phonon interactions on the one-electron states of solids. In *Solid State Physics*; Frederick Seitz, D. T., Ehrenreich, H., Eds.; Academic Press: New York, 1970; Vol. 23, pp 1–181.